

# Reconstruction of former glacier surface topography from archive oblique aerial images



N.G. Midgley<sup>a,\*</sup>, T.N. Tonkin<sup>a,b</sup>

<sup>a</sup> School of Animal, Rural and Environmental Sciences, Nottingham Trent University, Brackenhurst Campus, Southwell, Nottinghamshire NG25 0QF, UK

<sup>b</sup> Department of Natural Sciences, University of Derby, Kedleston Road, Derby DE22 1GB, UK

## ARTICLE INFO

### Article history:

Received 28 July 2016

Received in revised form 4 January 2017

Accepted 4 January 2017

Available online 06 January 2017

### Keywords:

Structure-from-Motion

Glacier change

Oblique aerial imagery

Surge-type glaciers

Midtre and Austre Lovénbreen, Svalbard

## ABSTRACT

Archive oblique aerial imagery offers the potential to reconstruct the former geometry of valley glaciers and other landscape surfaces. Whilst the use of Structure-from-Motion (SfM) photogrammetry with multiview stereopsis (MVS) to process small-format imagery is now well established in the geosciences, the potential of the technique for extracting topographic data from archive oblique aerial imagery is unclear. Here, SfM-MVS is used to reconstruct the former topography of two high-Arctic glaciers (Midtre and Austre Lovénbreen, Svalbard, Norway) using three archive oblique aerial images obtained by the Norwegian Polar Institute in 1936. The 1936 point cloud was produced using seven LiDAR-derived ground control points located on stable surfaces in proximity to the former piedmont glacier termini. To assess accuracy, the 1936 data set was compared to a LiDAR data set using the M3C2 algorithm to calculate cloud-to-cloud differences. For stable areas (such as nonglacial surfaces), vertical differences were detected between the two point clouds (RMS M3C2 vertical difference of 8.5 m), with the outwash zones adjacent to the assessed glacier termini showing less extensive vertical discrepancies (94% of M3C2 vertical differences between  $\pm 5$  m). This research highlights that historical glacier surface topography can be extracted from archive oblique aerial imagery, but accuracy is limited by issues including the lack of camera calibration, the quality and resolution of the archive imagery, and by the identification of suitable ground control. To demonstrate the value of historical glacier surfaces produced using oblique archive imagery, the reconstructed glacier surface topography is used to investigate evidence of a potential former surge front at the high-Arctic valley glacier, Austre Lovénbreen – a glacier identified to have potentially exhibited surge-type behaviour during the Neoglacial. A surface bulge of ~15–20 m is resolved on the 1936 model; however, when compared with the now deglaciated former subglacial topography, a surge origin for the surface feature becomes unclear. The processed 1936 oblique imagery was also used to produce orthorectified nadir aerial imagery, from which structural mapping was undertaken: this adds to the existing 1948–1995 structural map series for these glaciers. This research demonstrates the potential of SfM-MVS for reconstructing historical glacier surfaces, which is important for aiding our understanding of former glacier dynamics and enabling the rapid assessment of glacier change over time.

© 2017 The Authors. Published by Elsevier B.V. This is an open access article under the CC BY-NC-ND license (<http://creativecommons.org/licenses/by-nc-nd/4.0/>).

## 1. Introduction

The aim of this research is to demonstrate the use of archive oblique aerial imagery to reconstruct glacier surface topography using Structure-from-Motion with multiview stereopsis (SfM-MVS). This research is important because the technique has the potential to aid our understanding of early twentieth century glacier change prior to the period of the direct measurement of glaciers in the second half of the twentieth century. The potential of this technique is significant given the vast archives of underutilised early twentieth century imagery. The record of glacier change obtained from direct measurement, as published by the

World Glacier Monitoring Service (WGMS, 2015), is concentrated within the second half of the twentieth century. For example, in Svalbard, records of glacier mass balance extend back to the 1950s (Hagen and Liestøl, 1990), but are restricted to a few study sites. Nadir aerial imagery (i.e. imagery obtained from an aerial platform with a view straight down) is often used to extend glacier records prior to the period of direct mass balance and satellite monitoring (Bjørk et al., 2012; Kjær et al., 2012; Kjeldsen et al., 2015). Kjeldsen et al. (2015) used archive nadir aerial images to produce glacier DEMs of outlet glaciers from the Greenland Ice Sheet, highlighting the potential of archive aerial photography for glaciological monitoring.

Whilst nadir imagery is commonly used, oblique aerial imagery can also be used for similar purposes, although the extraction of topographic data is limited by the viewshed (visibility) of each image. In Svalbard,

\* Corresponding author.

E-mail address: [nicholas.midgley@ntu.ac.uk](mailto:nicholas.midgley@ntu.ac.uk) (N.G. Midgley).

the Norwegian Polar Institute collected oblique aerial imagery in 1936 and 1938 to produce the first accurate maps of Svalbard at a scale of 1:100,000 with topography presented as 50-m contours (Nuth et al., 2007, 2013). The 1936/38 topographic data set is often used by glaciologists as a historical data set for estimating twentieth century glacier volume change (e.g., Kohler et al., 2007; Sund et al., 2009; Lapazaran et al., 2013). Specifically, Nuth et al. (2007) used the 1936 topographic data to calculate a 16% reduction in glacier coverage between 1936 and 1990 for western and central regions in Svalbard. Kohler et al. (2007) used the 1936 topography to calculate long-term glacier change at Slakbreen and Midtre Lovénbreen. Midtre Lovénbreen was calculated to be thinning at an accelerated rate from 2003 to 2005 compared to the 1936–1962 study period (Kohler et al., 2007). However, difficulty in using this oblique aerial imagery was highlighted by James et al. (2012).

Oblique aerial imagery also provides an opportunity to study glacier dynamics, including assessment of surge-type behaviour, locating glacier frontal positions, and interpreting the significance of glacier structures (e.g., Dowdeswell and Benham, 2003; Glasser et al., 2004; Hambrey et al., 2005; Kristensen and Benn, 2012; Midgley et al., 2013).

Whilst the use of SfM-MVS for close range and small-format aerial image processing is now commonplace (e.g., Westoby et al., 2012; Tonkin et al., 2014, 2016; Nolan et al., 2015; Ryan et al., 2015), few studies have used SfM-MVS for the purposes of producing orthorectified imagery and surface models from archive nadir aerial imagery (Gomez et al., 2015; Ishiguro et al., 2016; Tonkin et al., 2016). With the exception of Frankl et al. (2015), published case studies that solely report on the effectiveness of SfM-MVS for processing archive oblique aerial imagery are rare. This photogrammetric technique has potential benefits as the camera pose and scene geometry are all automatically calculated using iterative algorithms (Westoby et al., 2012). For archive imagery, where camera information is missing (but ground control can be applied if areas of unchanged surface topography exist), quantitative data can be rapidly extracted where imagery is sufficiently overlapping. This allows for a dense cloud of points to be generated using multiview stereo reconstruction. Eltner et al. (2016) and Smith et al. (2015) provide excellent reviews of the technique and its recent geoscientific applications. Whilst the application of photogrammetry in glaciology has a long history (e.g., Finsterwalder, 1931; Finsterwalder, 1954; Fox and Nuttall, 2007; Kjeldsen et al., 2015; King et al., 2016), uncertainty remains regarding whether the SfM-MVS method can produce data of an appropriate quality to benefit our understanding of former glacier characteristics. Furthermore, the processing of archive oblique aerial imagery

is of interest not only for understanding long-term glacier response in Svalbard but also for areas such as North America, Greenland, the Antarctic, and Himalaya, where the scientific potential of oblique image archives are yet to be realised. Methods for utilising oblique aerial image sets for glaciological applications are needed; thus, in this study the effectiveness of the SfM-MVS workflow for this purpose is investigated.

## 2. Study site

The potential of the SfM-MVS method applied to archive oblique aerial imagery is explored using Midtre and Austre Lovénbreen as examples. These two small (currently ca. 4-km-long glaciers, but previously ca. 5-km-long at the Neoglacial maximum) valley glaciers are located on Brøggerhalvøya, northwest Spitsbergen, in the Svalbard archipelago (Fig. 1). The likely Neoglacial maximum extent of Midtre Lovénbreen was photographed by Hamberg (1894) in 1892 CE (the image was also reproduced by Hambrey et al., 2005). The mass balance record of Midtre Lovénbreen dates back to 1968, with currently published data to 2013 (WGMS, 2015) and shows a negative mass balance over the observation period with the exception of only four years. Svalbard experiences a relatively mild climate for its latitude. For example, nearby Ny-Ålesund (ca. 5 km from the two glaciers) experienced a mean annual temperature of  $-6.3^{\circ}\text{C}$  from 1961 to 1990 and  $-5.2^{\circ}\text{C}$  from 1981 to 2010 (Førland et al., 2011). Midtre and Austre Lovénbreen have been subject to debate regarding the potential for surge-type behaviour. Jiskoot et al. (2000) suggested that Midtre Lovénbreen was not surge type, whereas Hansen (2003) suggested that it had surged in the past but could no longer be classified as a surge-type glacier. Hambrey et al. (2005) also concluded that Midtre Lovénbreen was either not a surge-type glacier, or at least had not surged for several hundred years. However, King et al. (2008) suggested that the character of the basal material would not support fast glacier flow. The nearby Pedersenbreen has very clear evidence of repeated surge activity (Glasser et al., 2004). A potential surge front was reported based upon the visual assessment of the oblique aerial imagery taken by the Norwegian Polar Institute in 1936, on the adjacent Austre Lovénbreen (Midgley et al., 2013). A steep surge front has been identified at other glacier surges (e.g., Murray et al., 1998; King et al., 2016) and is, therefore, a potential diagnostic feature of surge activity. Farnsworth et al. (2016) reported Austre Lovénbreen as a potential surge-type glacier by using the presence of crevasse-squeeze ridges as

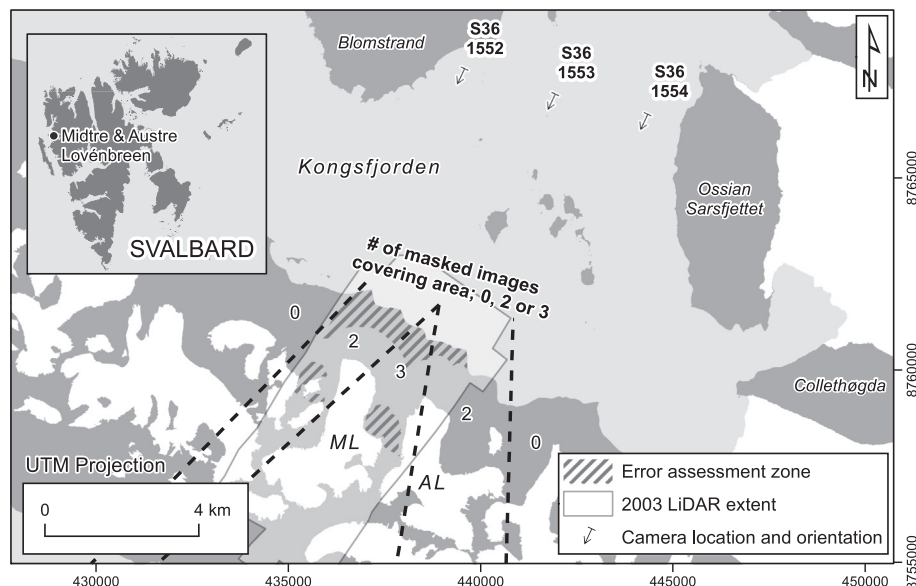


Fig. 1. The location of Midtre Lovénbreen (ML) and Austre Lovénbreen (AL), Svalbard, and the locations of the images used to reconstruct the 1936 glacier surface topography.

an indicator of former surge activity. Here, using archive oblique imagery of Midtre and Austre Lovénbreen, the former (1936) surfaces of Midtre Lovénbreen and Austre Lovénbreen are investigated for evidence of surge-type behaviour using SfM-MVS data generated by this research.

### 3. Methods

#### 3.1. Model generation

Three oblique aerial images of Brøggerhalvøya (Table 1), obtained by the Norwegian Polar Institute (NPI) in 1936 (positions delimited in Fig. 1), were processed using SfM-MVS software (Agisoft PhotoScan, v. 1.2.3) to produce a dense point cloud of the surface and an orthorectified image of area covering parts of Midtre and Austre Lovénbreen and the surrounding area. The oblique images were captured at an altitude of ~3000 m using a Zeiss RMK P21/18 camera with a nominal focal length of 21 cm and image size of  $18 \times 18$  cm (Aas, pers comms.). The scanned images have a resolution of 1841 dpi ( $12,962 \times 12,970$  pixels); however, the clarity of the images is reduced by minor blurring on the scanned images. Given the oblique nature of the imagery, the ground resolution of the imagery varies from 0.42 to 0.44 m per pixel along the coastline and increases to 0.50–1.77 m per pixel along the glacier midpoints. The foreground of each image includes a field of view of around 5 km, whereas the background of each image includes a field of view in excess of 50 km (Fig. 2). The image processing workflow involves: (i) undertaking an image quality check; (ii) the application of a mask over unwanted parts of the scanned images; (iii) alignment of images using the high accuracy and generic pair preselection setting; (iv) building of the dense point cloud using the medium quality point setting; (v) building of the mesh from the dense point cloud and height field surface type, which is optimised for aerial images; and (vi) texture produced using the generic setting. The image quality check reports a value between 0 and 1 and images with quality values under 0.5 should be discarded from the processing workflow. The image quality values of the three images processed were assessed as 0.61, 0.62, and 0.64, which is below the 0.7 quality threshold that the authors have adopted elsewhere for contemporary low-level, small-format aerial imagery (e.g., Tonkin and Midgley, 2016). As the area of interest was only covered by a small proportion of each image (<26%; Fig. 2; Table 1), a mask was applied to each image to exclude areas beyond the study area and the fiducial markers from the processing (e.g., water bodies such as Kongsfjorden). The resulting scene was reconstructed using 3500 tie points between the three images, with the peripheral areas of the scene reconstructed from two images and the central area from three images (Fig. 1). The medium point density setting was found to produce the highest density point cloud results (~2.8 million points) as the software was unable to produce a usable point cloud with the high point density setting. After Barrand et al. (2009), ground control coordinates were derived from an existing LiDAR data set that was collected in 2003 by the Natural Environment Research Council Airborne Research Survey Facility (NERC ARSF). As reported by Barrand et al. (2009), the LiDAR data density varies according to scan height and the presence of swath overlaps

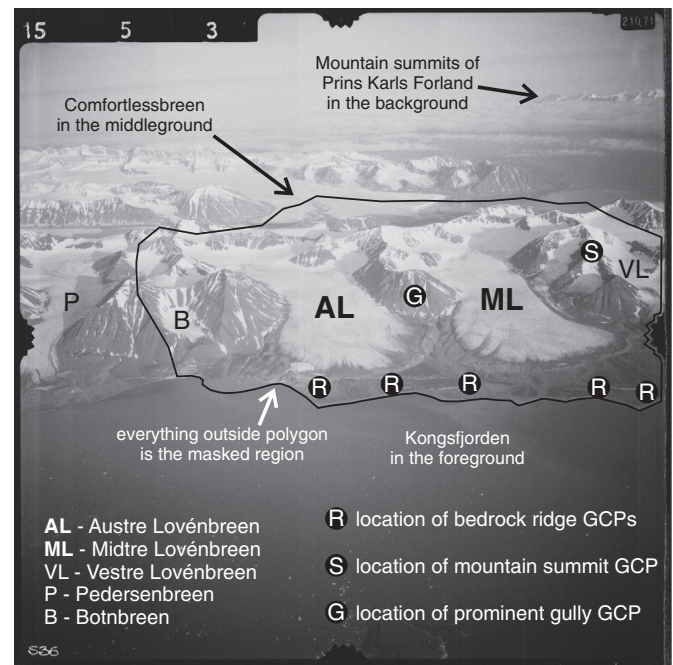


Fig. 2. Example image used for surface reconstruction showing the masked area, location of ground control points, and identification of Midtre Lovénbreen (ML) and Austre Lovénbreen (AL). Aerial photograph S36 1553 is published with permission of the Norwegian Polar Institute.

with an estimated  $\sim 1.15$  points  $m^{-2}$  spatial resolution over the entire data set. The LiDAR data set is not error free, but a likely error of around  $\pm 0.2$  m gives confidence that it provides a usable data set for comparison. The distribution of ground control (thus area of interest) was limited to the extent of the LiDAR point cloud, which covered the entirety of Midtre Lovénbreen, and the western terminus of Austre Lovénbreen. The location and spatial distribution of ground control points were determined by the identification of prominent features that have undergone limited change between the 1936 imagery and the 2003 LiDAR. This meant that a large part of the image scene, such as the glacier surface, the outer-frontal moraine complexes, and the proglacial outwash were unsuitable for ground control location. A total of seven ground control points were used, two of which were located on a mountainside and mountain summit and five of which were located on bedrock ridges found outside the Neoglacial maximum extent of Austre and Midtre Lovénbreen (Fig. 2). Ground control points were identified on either two or three images depending on the degree of overlap (Fig. 1). Once the model was optimised, the total RMS (root-mean-square) error for these ground control points was 4.5 m.

#### 3.2. Accuracy assessment of the 1936 surface model

Validation of the SfM-MVS derived surface model was conducted by using points from 'stable terrain' (e.g., the relatively stable nonglacial

Table 1  
Image details and camera locations.

1936 image ID	Field of view along coastline (km)	Approximate ground resolution (m per pixel)		% of image used	Estimated camera position (m)			Distance to area of interest (km)
		Coastline	Glacier mid-point		X <sup>a</sup>	Y <sup>a</sup>	h <sup>b</sup>	
S36_1552	~5.4	0.42	1.77	23	439,498	8,767,652	3125	~8
S36_1553	~6.5	0.50	0.61	26	441,850	8,766,989	3104	~8
S36_1554	~7.5	0.58	0.65	17	444,257	8,766,464	3125	~9

<sup>a</sup> UTM projection.

<sup>b</sup> Ellipsoid height.

surfaces) located on fixed bedrock areas, and from mountain sides adjacent to the glaciers of interest (Fig. 1). This was conducted by comparing the NERC 2003 LiDAR point cloud to the dense point cloud produced using SfM-MVS with the 1936 images. A range of approaches have been adopted for validating SfM data (Smith and Vericat, 2015), each of which has merits and drawbacks (Carrivick et al., 2016). Here, the M3C2 (Multiscale Model to Model Comparison) plugin by Lague et al. (2013) was used, with the analysis undertaken in CloudCompare (v. 2.6.2); an open source three-dimensional point cloud software package. The M3C2 calculates the mean cloud-to-cloud difference and can be undertaken for surface normal directions where they can be robustly calculated (e.g., Lague et al., 2013; Westoby et al., 2016). However, here, only vertical directions were analysed as a measure of disagreement between the 1936 SfM-MVS point cloud and the reference LiDAR data set. This analysis is analogous to gridded DEM analysis (Lague et al., 2013) but has the benefit of comparing the raw point clouds, circumventing additional uncertainty associated with DEM production. Furthermore, a limited viewshed will generate excessively interpolated topographic data (e.g., Westoby et al., 2012). By only comparing the point clouds, only areas where topography can be reconstructed are compared, thus reducing apparent error associated with interpolation error. As much of the landscape has undergone significant alteration over the course of the twentieth century, nonglacial surfaces were compared to estimate vertical differences on the resulting reconstructed topographic data (Fig. 1). These areas covered the outwash plains in front of Midtre and Austre Lovénbreen, a series of bedrock ridges and the camera-facing flanks of mountains adjacent to the two glaciers (Fig. 1). To assess the horizontal accuracy of the orthorectified image output, a qualitative comparison was made between fixed landscape features visible on the NP Ortofoto Svalbard WMTS 25833 layer provided by the Norwegian Polar Institute (NPI).

### 3.3. Structural glaciological mapping from 1936 orthorectified imagery at Austre and Midtre Lovénbreen

Glacier surface features were mapped in a similar manner to that of Hambrey et al. (2005) who documented the structural glaciology of Midtre Lovénbreen in 1948, 1966, 1971, and 1995 but were unable to map features from the 1936 oblique imagery. The structures mapped by Hambrey et al. (2005) included primary stratification, longitudinal foliation, crevasse traces, arcuate upglacier-dipping fractures, and longitudinal splaying fractures in the terminus area. Here, these features were mapped as linear units from the orthorectified aerial imagery within ArcGIS 10.3.1. The contrast and brightness of the raster data sets were manipulated to aid identification of structures from the raster data sets. Linear structural units were mapped and interpreted on the basis of feature form and spatial distribution.

## 4. Results

### 4.1. Accuracy assessment of the 1936 SfM-MVS data

The stable areas located in the outwash zones adjacent to the glacier termini provided an RMS vertical M3C2 difference of 2.9 m, with 94% of M3C2 vertical distances within  $\pm 5$  m (Fig. 3; Table 2). The vertical differences in the proglacial zone are negatively skewed, with a mean difference of  $-0.8$  m ( $\sigma = 2.9$  m) highlighting that, on average, the reproduced 1936 topographic data falls below the reference data set in this area. Including mountain sides within the analysis area yielded an increased RMS vertical M3C2 difference of 8.5 m and a mean M3C2 difference of 0.5 m ( $\sigma = 8.5$  m). Areas of vertical disagreement (i.e. where the reconstructed 1936 topography is vertically lower than the reference LiDAR data set) include mountain

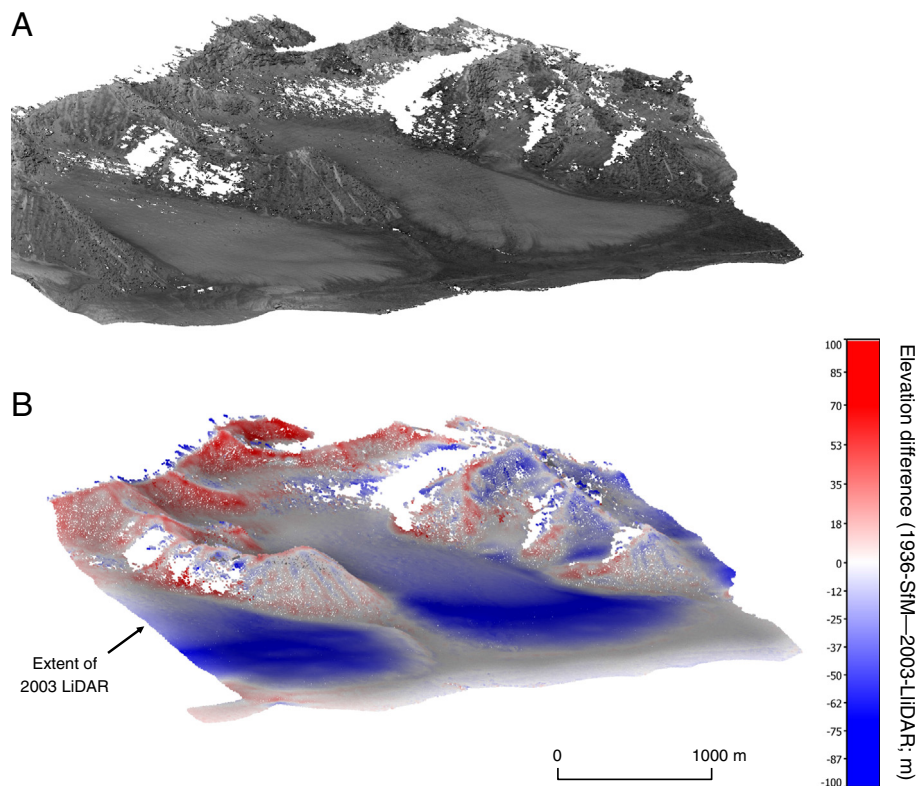


**Fig. 3.** (A) A point cloud generated from three 1936 oblique aerial images using SfM-MVS. The cloud contains ~2.8 million points. (B) Vertical difference between the 1936 point cloud and the reference NERC 2003 LiDAR data. Red represents positive vertical difference between the 1936 SfM-MVS data set and the reference 2003 LiDAR data set; whereas blue shows a negative vertical difference. The recession of Austre and Midtre Lovénbreen between 1936 and 2003 is clearly constrained by this analysis. (For interpretation of the references to colour in this figure legend, the reader is referred to the web version of this article.)

**Table 2**  
Summary table assessing vertical differences between stable nonglacial areas of the 1936 surface against NERC 2003 LiDAR data.

Area	Number of M3C2 vertical distances	Vertical difference (m)			%				
		Mean difference	Standard deviation	Root-mean-square	Min	Max	± 5 m	± 10 m	± 20 m
Outwash/bedrock	6474	−0.8	2.8	2.9	−26.5	25.3	94	99	100
Mountain sides	15,273	3.6	14.5	14.9	−77.9	109.9	29	56	87
All 'stable' areas	21,747	0.5	8.5	8.5	77.9	109.9	75	86	99

sides and summits where vertical differences exceed 10 m. Assessed separately, mountain sides show considerably greater variation than other assessed 'stable' areas (Table 2).

The orthorectified imagery appears to be well aligned with an NPI orthorectified aerial image with displacements typically < 10 m. This is highlighted in Fig. 4, which shows a series of features on modern NPI orthorectified imagery and on the orthorectified 1936 imagery produced here. Also worth noting is that the NPI data set used for this comparison will not be error free. The direction that the imagery is displaced varies across the imagery, largely relating to local deformations caused by the distribution of ground-control points applied during the image processing.

#### 4.2. Structural glaciological mapping from 1936 orthorectified imagery at Austre and Midtre Lovénbreen

The orthorectified imagery provides an opportunity to map the distribution of structural features present on Austre and Midtre Lovénbreen (Fig. 5). Arcuate structures transverse to glacier flow are identified up-glacier of the piedmont terminus on Midtre Lovénbreen. Similar structures are less readily identified on Austre Lovénbreen because of the poorer image texture on the orthophoto used for structural mapping. Additional transverse to flow features occur in proximity to the glacier termini of Austre and Midtre Lovénbreen; however, unlike transverse features located up-glacier, the transverse to flow features in proximity to the glacier termini are less intensely folded. In places, the transverse features in proximity to the termini appear to be debris bearing, resulting in discrete accumulations of supraglacial debris.

Linear features, which run approximately parallel to glacier flow, are also identified in proximity to the termini of Austre and Midtre Lovénbreen. On Austre Lovénbreen, one such feature appears to be deformed in proximity to a surface bulge on the glacier surface on the left of the glacier (Fig. 5).

The termini of both glaciers contact the Neoglacial moraine ramparts and are debris-laden, with debris stripes located down-glacier of linear features running parallel to the direction of flow. Additional supraglacial debris in the form of a medial moraine are located on the left side of Midtre Lovénbreen, originating from the confluence between two flow units, including a small cirque basin that has subsequently detached from the main glacier terminus (Hambrey et al., 2005).

#### 4.3. Assessment of glacier topography

Profiles across the former 1936 surfaces of Midtre and Austre Lovénbreen, as reconstructed from the oblique aerial imagery, are shown in Fig. 6. Based on the SfM-MVS reconstruction, both glaciers attained a termini ice thickness of up to ~80 m in 1936. In contrast to Midtre Lovénbreen, an ~15–20 m high (at ~300–600 m along the profile) surface bulge was resolved by the SfM-MVS process on the surface of Austre Lovénbreen – a feature that was previously interpreted as a potential surge front by Midgley et al. (2013). By analysing the glacier surface, as reconstructed by the SfM-MVS process alongside the 2003 LiDAR data set, the relationship between the surface and subglacial topography can be assessed. At ~300 m along the 2003 profile, a 30-m drop in former subglacial elevation can be seen (Fig. 6). This drop in surface elevation is also mirrored by the reconstructed 1936 glacier surface.

## 5. Discussion

### 5.1. Effectiveness of SfM-MVS for reconstructing former glacier surfaces

A number of factors contribute to the quality of the resulting reconstructed topography. Ground control is a principal requirement for producing georeferenced data using the SfM-MVS technique and is critical if the resulting point cloud and derivative data are to accurately represent the reproduced surface. Suitable ground control features need to be identified on multiple image sets. Here, the poor quality imagery (PhotoScan image quality values of 0.61, 0.62, and 0.64) was found to limit the identification of suitable features that could be used for ground control. Unlike nadir imagery, where features such as mountain summits and ridges are more readily identified (e.g., Barrand et al., 2009) with distance from the camera, features on the oblique imagery are less well defined. Here, seven ground control points of sufficient quality on the imagery were used to produce the SfM-MVS data set. This contrasts with the work of Barrand et al. (2009), where up to 50 ground control points were used to obtain low error on a nadir image set collected by the NERC ARSF in 2003. For the NPI imagery, robust ground control is more likely to be identified in the foreground of the imagery, leaving parts of the reconstructed scene (e.g., the accumulation areas of the glaciers) unconstrained.

Despite the preferential selection of ground control locations in the foreground of the imagery, which were covered in greater detail owing to the oblique nature of the imagery, the quality of the imagery results in suboptimal ground control identification and placement. Fixed features can be blurred or poorly distinguished in the source imagery resulting in potential errors of around 5 m – an issue that is inherent to the quality of the archive oblique imagery used. Error results from high-precision coordinate values (e.g., centimetre precision) being applied to 'points' on the imagery that are several metres across or poorly defined. For small-format aerial imagery, poorly distributed ground control points have been linked to degraded surface reconstruction (e.g., Clapuyt et al., 2016; Tonkin and Midgley, 2016) – an issue that will also affect the quality of topographic data produced from archive imagery. A further issue relates to the dynamic nature of the high-Arctic environment where features (e.g., most surfaces with the exception of bedrock) in the landscape are unlikely to be fixed over long periods because of degrading permafrost and glacier recession. Ground control points are, therefore, limited to stable (nonglacial) locations within the image scene, which may leave large areas of the surface model unconstrained and subject to potential error. Vertical difference increased when the mountain sides were included, most likely caused by poorly constrained topography because of a limited viewshed, shading, and steep terrain. The association between slope and topographic error is well established. For example, Nuth et al. (2007) found that horizontal mismatches between the 1936 contour map and 1990 NPI DEM promoted vertical differences, which were exaggerated on steep terrain.

Ground control was located in excess of 7 km from the reconstructed camera positions (Table 1), with the immediate foreground of the imagery covering water (Fig. 2; Kongsfjorden) and with the background field of view exceeding 50 km, making large parts of the imagery redundant for the application of ground control. The 7 km distance between camera location and ground control location is by far in excess of the typical distance undertaken for nadir aerial

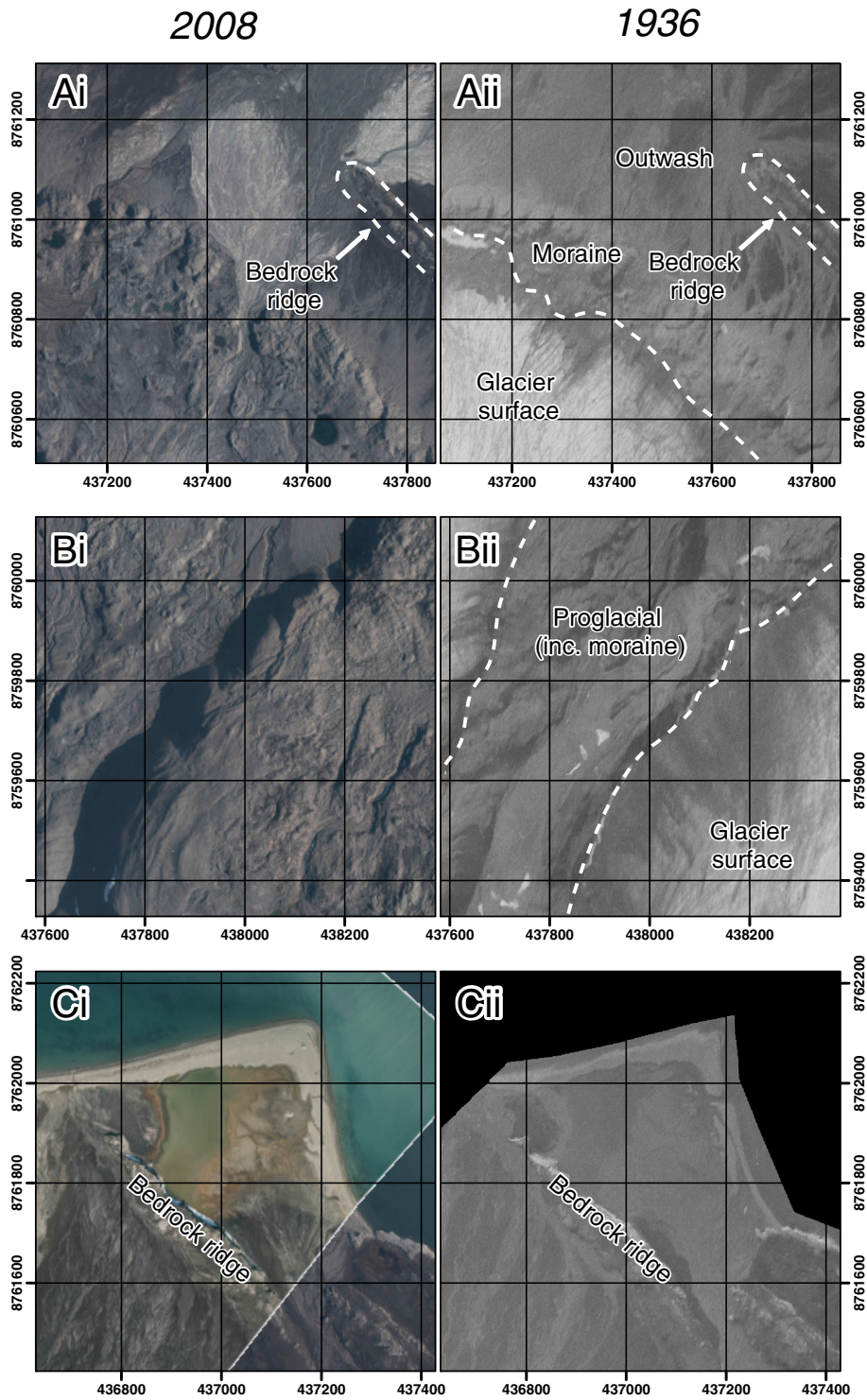


**Fig. 4.** Samples of 2008 orthorectified imagery from the Norwegian Polar Institute and 1936 orthorectified imagery generated using the SfM-MVS approach. (Ai) The deglaciaded proglacial area of Midtre Lovénbreen and associated moraine in 2008. (Aii) The same location in 1936 highlighting the former position of the glacier terminus. (Bi) Ice-cored moraine on the left lateral margin of Austre Lovénbreen in 2008. (Bii) The same position location in 1936 where the glacier terminus can be seen abutting the moraine. (Ci and Cii) A bedrock ridge and coastal bar located on the outwash plain.

imagery, where the camera positions typically are located closer to the reconstructed surface (e.g., 1.6 km; Arnold et al., 2006; Barrand et al., 2009). Despite this, the findings demonstrate that ground control can be applied to archive oblique imagery of this type; however, lower error resulting from this source would be permitted where camera positions are located in closer proximity to the reconstructed

scene. Survey range appears to be a key control on the quality of surface reconstruction (Smith and Vericat, 2015). For example, in a recent study by Mosbrucker et al. (in press), 67 SfM data sets were analysed, with the authors reporting that 'nominal ground sample distance' as a variable explains 68% of the variability in mean absolute vertical error. As such, the variable ground sample distance

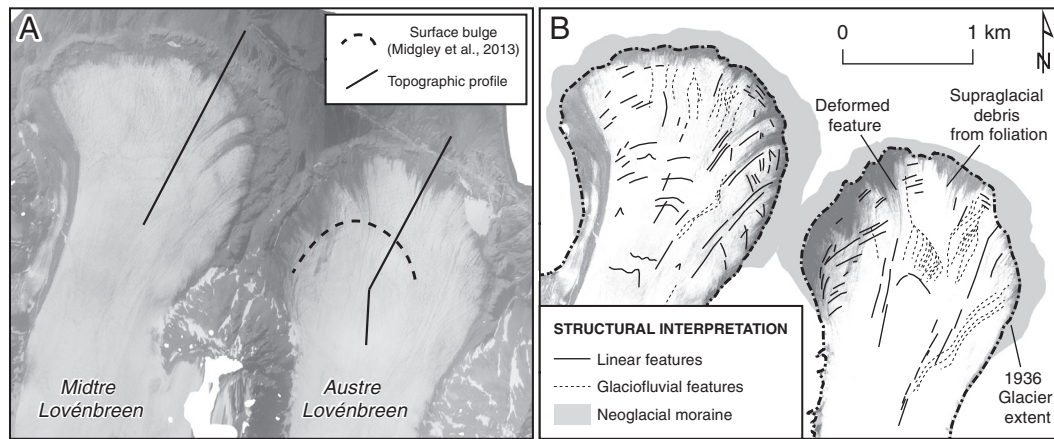


Fig. 5. Structural glaciological interpretation of Austre and Midtre Lovénbreen (1936).

(Table 1) on the oblique archive imagery used here will contribute to error on the resulting data and limits the achievable accuracy of this approach.

Despite these issues, the results indicate that aerial imagery can be successfully used to reconstruct former glacier topography, with expected vertical accuracies typically within 10 m (Table 2). Whilst the original 1936 contour map has provided a reference data set for assessing long-term glacier change (Kohler et al., 2007; Sund et al., 2009; Lapazaran et al., 2013), SfM-MVS processing of the oblique imagery provides significantly greater detail for glaciological applications. Nuth et al. (2007) highlighted an average elevation difference of  $-3.1$  m ( $\sigma = 12.2$  m) for nonglacier land elevation differences when the digitised 1936 data set was compared to the 1990 NPI DEM. Although the reconstructed topography presented here only represents a small proportion of the study area of Nuth et al. (2007), the results provide average elevation difference of  $-0.6$  m ( $\sigma = 9.6$  m), demonstrating that the reprocessing of archive oblique aerial imagery should

result in an increase in accuracy compared to digitised contours. Furthermore, Nuth et al. (2007) highlighted that some contours on the original 1936 data were estimated and hand drawn where visibility of landscape features (e.g., areas obscured by mountains) was insufficient. By using SfM-MVS, a point cloud and surface can be produced rather than previous approaches that have digitised polylines from historical maps that require interpolation to produce a surface. Where aerial imagery is reprocessed, areas of topography less confidently reconstructed can be readily identified and a better understanding of error obtained, circumventing issues related to estimated hand-drawn contours. Here, topography was resolved from three images, with part of the scene reconstructed from only two overlapping images. The results highlight that oblique stereo image pairs can be used to extract geometric information using SfM-MVS, although additional imagery is preferable.

The potential to extract topographic data from archive imagery using this approach is clear; however, the purpose for which the data is used needs to be assessed alongside the error levels. Error, which is

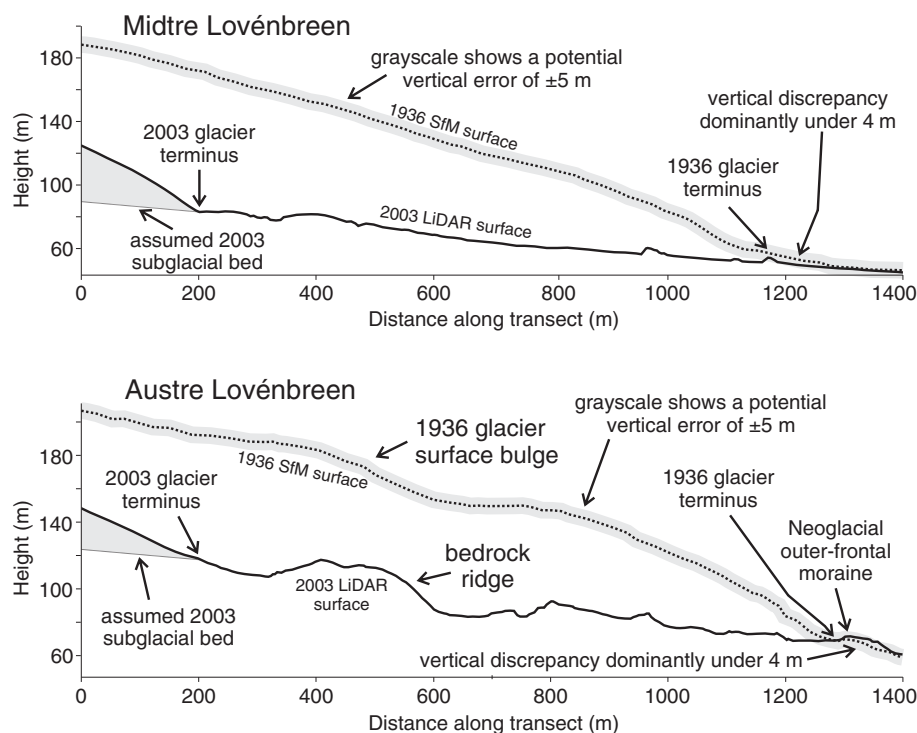


Fig. 6. Profiles of the glacier termini surfaces of Austre and Midtre Lovénbreen in 1936 and the subglacial topography based on the NERC 2003 LiDAR data set.

inherent to all topographic data, limits the application of this technique for estimating changes smaller than the magnitude of error. Despite this, areas such as glacier termini are well resolved by the SfM-MVS process, with glacier change captured between the 1936 SfM-MVS data set and the 2003 LiDAR ‘reference’ data set, demonstrating the high fidelity with which former surfaces can be reconstructed. Given the effectiveness of SfM-MVS for the extraction of topographic data from archive oblique aerial imagery, future research investigating whether the technique can also be applied to terrestrial image archives for the purpose of historical glacier reconstruction is logical.

Small-scale topographic features on the glacier surface can be resolved by the SfM-MVS process allowing the morphometric statistics to be calculated. In the example investigated here, SfM-MVS derived data aid the interpretation of former glacier dynamics. The SfM-MVS method also provides an opportunity for oblique imagery to be used to identify and map former structural glaciology, providing insight into the dynamic response of glaciers over time. Hambrey et al. (2005) highlighted that the oblique nature of the 1936 original imagery made it difficult to observe and map glacier structures. Here, by producing orthorectified imagery from only three images along the 1936 flight plan, a range of glaciological structures on the 1936 surface of Austre and Midtre Lovénbreen were mapped (Fig. 6).

### 5.2. Interpretation of structural glaciology from 1936 orthorectified imagery at Austre and Midtre Lovénbreen

The interpretation of structural glaciology is based on the spatial distribution and orientation of mapped features. As the flow-parallel features occur down-glacier of folded structures running approximately transverse to glacier flow (Fig. 5), the features primarily signify the transposition of layering (stratification) that becomes progressively folded down-glacier into longitudinal foliation parallel to ice flow. The presence of foliation and folding of primary layering highlight strong lateral compression at both glaciers. The locations of these mapped feature are consistent with longitudinal foliation structures that typically occur at the confluence between flow units and in areas of lateral compression (related to the topographic controls on glacier geometry; Hambrey and Lawson, 2000; Roberson, 2008; Jennings et al., 2014), with the debris component relating to the incorporation of passively transported rock-fall debris at the accumulation basins of Austre and Midtre Lovénbreen (Hambrey et al., 1999).

Transverse features occurring in proximity to the glacier termini are interpreted as fractures including thrusts after Hambrey et al. (2005), who identified similar features at Midtre Lovénbreen using uncorrected nadir imagery from 1948, 1966, and 1995. The propagation of debris from these features onto the glacier surface provides evidence of the down-wastage of Midtre and Austre Lovénbreen since the Neoglacial maximum that occurred ca. 1900 (Hambrey et al., 2005). Critically, open crevasses are not visible on the imagery, suggesting that by 1936 Midtre and Austre Lovénbreen had responded significantly to ameliorating twentieth century conditions (e.g., Hambrey et al., 2005; Lovell et al., 2015) resulting in reduced dynamism and ice stagnation.

### 5.3. Is there evidence of a surge front propagating down Austre Lovénbreen in 1936?

The surge type character of glaciers on Brøggerhalvøya has been debated (e.g., Jiskoot et al., 2000; Hansen, 2003; Glasser et al., 2004; King et al., 2008). Midgley et al. (2013) identified a surface bulge, which was suggested could relate to a surge front on the surface of Austre Lovénbreen, based upon the interpretation of a single oblique 1936 aerial image. Here, the surface bulge is resolved by the SfM-MVS method; however, when assessed alongside the 2003 topographic data, doubt is cast on the validity of this interpretation. Specifically, the topography of the glacier surface appears to mirror that of the subglacial topography below the former bulge (Fig. 6). Whether the surface bulge simply

reflects glacier flow over subglacial topography or represents the remnants of a former surge front propagating down Austre Lovénbreen in 1936 is, therefore, unclear.

Farnsworth et al. (2016) mapped crevasse-squeeze ridges across Svalbard from aerial imagery, using the presence of the landforms as evidence for former surge-type glacier behaviour. However, the location of the crevasse-squeeze ridges mapped by Farnsworth et al. (2016) in the proglacial area of Austre Lovénbreen is unclear. As such, the surge-type character of Austre Lovénbreen remains uncertain. This work highlights that care must be taken when interpreting former glacier dynamics from archive imagery but also how modern SfM-MVS photogrammetric approaches can be used alongside recent topographic data sets to evaluate former glacier surfaces, especially where glaciers have receded sufficiently to allow for former subglacial topography to be mapped.

## 6. Summary and conclusions

The SfM-MVS method has huge potential for glaciologists wishing to visualise rapidly archive oblique imagery in three-dimensions. The technique, however, requires a number of issues to be considered prior to its application, such as the horizontal and vertical errors that may occur because of poor image quality, image resolution, and a limited spread of ground control points. These issues require consideration if quantitative measurements are required from the reconstructed geospatial data. Nevertheless, the technique is demonstrated to result in well-resolved topography with high fidelity, as demonstrated by limited vertical differences between the nonglacial areas on the 1936 data set and 2003 LiDAR point clouds (e.g., producing 94% of M3C2 vertical differences within  $\pm 5$  m for areas adjacent to the former glacier termini). Furthermore, this research demonstrates how the data reconstructed from archive oblique aerial images can be used to assess former dynamics and undertake structural mapping. Here, a surface bulge on the former 1936 surface of Austre Lovénbreen, which was previously linked to potential surge-type behaviour, was investigated in relation to the now exposed subglacial topography. Whilst Austre Lovénbreen may have exhibited surge-type behaviour over the Neoglacial, the ‘bulge’ investigated here is not conclusively linked to the propagation of a surge front in 1936 but might simply relate to the now exposed underlying bed topography. The structural mapping undertaken using the 1936 imagery adds to the existing 1948–1995 structural map series produced by Hambrey et al. (2005). In summary, the application of the SfM-MVS technique to archive oblique imagery offers an exciting avenue for geoscientific research, offering a low-cost and rapid method to extract topographic surface data and imagery from historical image sources and warrants further consideration.

## Acknowledgements

Dr. Harald Aas (Norwegian Polar Institute) is thanked for assistance with obtaining the archive imagery used in this research. Airborne LiDAR data from the UK Natural Environment Research Council (NERC) Airborne Research and Survey Facility (ARSF; now renamed Airborne Research Facility, ARF) are provided courtesy of NERC via the NERC Earth Observation Data Centre (NEODC). NGM and TNT gratefully acknowledge funding from Nottingham Trent University that enabled the completion and publication of this research. This manuscript also significantly benefited from comments provided by anonymous reviewers and Dr. Richard Marston.

## Appendix A. Supplementary data

Supplementary data associated with this article can be found in the online version, at [doi:10.1016/j.geomorph.2017.01.008](https://doi.org/10.1016/j.geomorph.2017.01.008). These data include the Google map of the most important areas described in this article.

## References

- Arnold, N.S., Rees, W.G., Hodson, A.J., Kohler, J., 2006. Topographic controls on the surface energy balance of a high Arctic valley glacier. *J. Geophys. Res.* 111, F02011. <http://dx.doi.org/10.1029/2005JF000426>.
- Barrand, N.E., Murray, T., James, T.D., Barr, S.L., Mills, J.P., 2009. Optimizing photogrammetric DEMs for glacier volume change assessment using laser-scanning derived ground-control points. *J. Glaciol.* 55 (189):106–116. <http://dx.doi.org/10.3189/002214309788609001>.
- Bjørk, A.A., Kjær, K.H., Korsgaard, N.J., Khan, S.A., Kjeldsen, K.K., Andresen, C.S., Box, J.E., Larsen, N.K., Funder, S., 2012. An aerial view of 80 years of climate-related glacier fluctuations in southeast Greenland. *Nat. Geosci.* 5:427–432. <http://dx.doi.org/10.1038/ngeo148>.
- Carrivick, J.L., Smith, M.W., Quincey, D.J., 2016. *Structure from Motion in the Geosciences*. Wiley-Blackwell, Oxford.
- Clapuyt, F., Vanacker, V., Van Oost, K., 2016. Reproducibility of UAV-based earth topography reconstructions based on Structure-from-Motion algorithms. *Geomorphology* 260:4–15. <http://dx.doi.org/10.1016/j.geomorph.2015.05.011>.
- Dowdeswell, J.A., Benham, T.J., 2003. A surge of Perseibreen, Svalbard, examined using aerial photography and ASTER high resolution satellite imagery. *Polar Res.* 22 (2): 373–383. <http://dx.doi.org/10.1111/j.1751-8369.2003.tb00118.x>.
- Eltner, A., Kaiser, A., Castillo, C., Rock, G., Neuring, F., Abellán, A., 2016. Image-based surface reconstruction in geomorphometry—merits, limits and developments. *Earth Surf. Dyn.* 4:358–389. <http://dx.doi.org/10.5194/esurf-4-359-2016>.
- Farnsworth, W.R., Ingólfsson, Ó., Retelle, M., Schomacker, A., 2016. Over 400 previously undocumented Svalbard surge-type glaciers identified. *Geomorphology* 264:52–60. <http://dx.doi.org/10.1016/j.geomorph.2016.03.025>.
- Finsterwalder, R., 1931. Geschwindigkeitsmessung an gletschern mittels photogrammetrie. *Z. Gletscherk.* 19, 251–262.
- Finsterwalder, R., 1954. Photogrammetry and glacier research with special reference to glacier retreat in the eastern Alps. *J. Glaciol.* 2, 306–314.
- Førland, E.J., Benestad, R., Hanssen-Bauer, I., Haugen, J.E., Skaugen, T.E., 2011. Temperature and precipitation development at Svalbard 1900–2100. *Adv. Meteorol.* 893790. <http://dx.doi.org/10.1155/2011/893790>.
- Fox, A.J., Nuttall, A.-M., 2007. Photogrammetry as a research tool for glaciology. *Photogramm. Rec.* 15 (89):725–737. <http://dx.doi.org/10.1111/0031-868X.00081>.
- Frankl, A., Seghers, V., Stal, C., De Maeyer, P., Petrie, G., Nyssen, J., 2015. Using image-based modelling (SfM-MVS) to produce a 1935 ortho-mosaic of the Ethiopian highlands. *Int. J. Digital Earth* 8 (5):421–430. <http://dx.doi.org/10.1080/17538947.2014.942715>.
- Glasser, N.F., Coulson, S.J., Hodkinson, I.D., Webb, N.R., 2004. Photographic evidence of the return period of a Svalbard surge-type glacier: a tributary of Pedersenbreen, Kongsfjord. *J. Glaciol.* 50 (169), 307–308.
- Gomez, C., Hayakawa, Y., Obanawa, H., 2015. A study of Japanese landscapes using structure from motion derived DSMs and DEMs based on historical aerial photographs: new opportunities for vegetation monitoring and diachronic geomorphology. *Geomorphology* 242:11–20. <http://dx.doi.org/10.1016/j.geomorph.2015.02.021>.
- Hagen, J.O., Liestøl, O., 1990. Long-term glacier mass-balance investigations in Svalbard. *Ann. Glaciol.* 14, 102–106.
- Hambrey, A., 1894. En resa till norra Ishafvet sommaren 1892. *Ymer* 14, 25–61.
- Hambrey, M.J., Lawson, W., 2000. Structural Styles and Deformation Fields in Glaciers: A Review. In: Maltman, A.J., Hubbard, B., Hambrey, M.J. (Eds.), *Deformation of Glacial Materials*. Geological Society, London, Special Publications Vol. 176:pp. 59–83. <http://dx.doi.org/10.1144/GSL.SP.2000.176.01.06>.
- Hambrey, M.J., Bennett, M.R., Dowdeswell, J.A., Glasser, N.F., Huddart, D., 1999. Debris entrainment and transfer in polythermal valley glaciers. *J. Glaciol.* 45 (149), 69–86.
- Hambrey, M.J., Murray, T., Glasser, N.F., Hubbard, A., Hubbard, B., Stuart, G., Hansen, S., Kohler, J., 2005. Structure and changing dynamics of a polythermal valley glacier on a centennial time-scale: Midre Lovénbreen, Svalbard. *J. Geophys. Res. Earth Surf.* F010006. <http://dx.doi.org/10.1029/2004JF000128>.
- Hansen, S., 2003. From surge-type to non-surge type glacier behaviour: Midre Lovénbreen, Svalbard. *Ann. Glaciol.* 36, 97–102.
- Ishiguro, S., Yamano, H., Oguma, H., 2016. Evaluation of DSMs generated from multi-temporal aerial photographs using emerging structure from motion—multi-view stereo technology. *Geomorphology* 268:64–71. <http://dx.doi.org/10.1016/j.geomorph.2016.05.029>.
- James, T.D., Murray, T., Barrand, N.E., Sykes, H.J., Fox, A.J., King, M.A., 2012. Observations of enhanced thinning in the upper reaches of Svalbard glaciers. *Cryosphere* 6: 1369–1381. <http://dx.doi.org/10.5194/tc-6-1369-2012>.
- Jennings, S.J., Hambrey, M.J., Glasser, N.F., 2014. Ice flow-unit influence on glacier structure, debris entrainment and transport. *Earth Surf. Process. Landf.* 39 (10): 1279–1292. <http://dx.doi.org/10.1002/esp.3521>.
- Jiskoot, H., Murray, T., Boyle, P.J., 2000. Controls on the distribution of surge-type glaciers in Svalbard. *J. Glaciol.* 46 (154), 412–422.
- King, E.C., Smith, A.M., Murray, T., Stuart, G.W., 2008. Glacier-bed characteristics of midre Lovénbreen, Svalbard, from high-resolution seismic and radar surveying. *J. Glaciol.* 54 (184):145–156. <http://dx.doi.org/10.3189/002214308784409099>.
- King, O., Hambrey, M.J., Irvine-Fynn, T.D., Holt, T.O., 2016. The structural, geometric and volumetric changes of a polythermal Arctic glacier during a surge cycle: Comfjellsbreen, Svalbard. *Earth Surf. Process. Landf.* 41 (2):162–177. <http://dx.doi.org/10.1002/esp.3796>.
- Kjær, K.H., Khan, S.A., Korsgaard, N.J., Wahr, J., Bamber, J.L., Hurkmans, R., van den Broeke, M., Timm, L.H., Kjeldsen, K.K., Bjørk, A.A., Larsen, N.K., Jørgensen, L.T., Færch-Jensen, A., Willerslev, E., 2012. Aerial photographs reveal late-20th-century dynamic ice loss in northwestern Greenland. *Science* 337:569–573. <http://dx.doi.org/10.1126/science.1220614>.
- Kjeldsen, K.K., Korsgaard, N.J., Bjørk, A.A., Khan, S.A., Funder, S., Larsen, N.K., Bamber, J.L., Colgan, W., van den Broeke, M., Siggaard-Andersen, M.L., Nuth, C., 2015. Spatial and temporal distribution of mass loss from the Greenland Ice Sheet since AD 1900. *Nature* 528 (7582):396–400. <http://dx.doi.org/10.1038/nature16183>.
- Kohler, J., James, T.D., Murray, T., Nuth, C., Brandt, O., Barrand, N.E., Aas, H.F., Luckman, A., 2007. Acceleration in thinning rate on western Svalbard glaciers. *Geophys. Res. Lett.* 34, L18502. <http://dx.doi.org/10.1029/2007GL030681>.
- Kristensen, L., Benn, D.I., 2012. A surge of the glaciers Skobreen-Paulabreen, Svalbard, observed by time-lapse photographs and remote sensing data. *Polar Res.* 31:11106. <http://dx.doi.org/10.3402/polar.v31i0.11106>.
- Lague, D., Brodu, N., Leroux, J., 2013. Accurate 3D comparison of complex topography with terrestrial laser scanner: application to the Rangitikei canyon (NZ). *ISPRS J. Photogramm. Remote Sens.* 82:10–26. <http://dx.doi.org/10.1016/j.isprsjprs.2013.04.009>.
- Lapazaran, J., Petlicki, M., Navarro, F., Machío, F., Puczkó, D., Glowacki, P., Nawrot, A., 2013. Ice volume changes (1936–1990–2007) and ground-penetrating radar studies of Ariebreen, Hornsund, Spitsbergen. *Polar Res.* 32:11068. <http://dx.doi.org/10.3402/polar.v32i0.11068>.
- Lovell, H., Fleming, E.J., Benn, D.I., Hubbard, B., Lukas, S., Naegeli, K., 2015. Former dynamic behaviour of a cold-based valley glacier on Svalbard revealed by basal ice and structural glaciology investigations. *J. Glaciol.* 61 (226):309–328. <http://dx.doi.org/10.3189/2015jogG14j120>.
- Midgley, N.G., Cook, S.J., Graham, D.J., Tonkin, T.N., 2013. Origin, evolution and dynamic context of a Neoglacial lateral-frontal moraine at Austre Lovénbreen, Svalbard. *Geomorphology* 198:96–106. <http://dx.doi.org/10.1016/j.geomorph.2013.05.017>.
- Mosbrucker, A.R., Major, J.J., Spicer, K.R., Pitlick, J., 2017. Camera system considerations for geomorphic applications of SfM photogrammetry. *Earth Surf. Process. Landf.* <http://dx.doi.org/10.1002/esp.4066> (in press).
- Murray, T., Dowdeswell, J.A., Drewry, D.J., Frearson, I., 1998. Geometric evolution and ice dynamics during a surge of Bakaninbreen, Svalbard. *J. Glaciol.* 44 (187), 263–273.
- Nolan, M., Larsen, C., Sturm, M., 2015. Mapping snow depth from manned aircraft on landscape scales at centimeter resolution using structure-from-motion photogrammetry. *Cryosphere* 9:1445–1463. <http://dx.doi.org/10.5194/tc-9-1445-2015>.
- Nuth, C., Kohler, J., Aas, H.F., Brandt, O., Hagen, J.O., 2007. Glacier geometry and elevation changes on Svalbard (1936–90): a baseline dataset. *Ann. Glaciol.* 46 (1):106–116. <http://dx.doi.org/10.3189/172756407782871440>.
- Nuth, C., Kohler, J., König, M., von Deschanden, A., Hagen, J.O., Kääh, A., Moholdt, G., Petterson, R., 2013. Decadal changes from a multi-temporal glacier inventory of Svalbard. *Cryosphere* 7:1603–1621. <http://dx.doi.org/10.5194/tc-7-1603-2013>.
- Roberson, S., 2008. Structural composition and sediment transfer in a composite cirque glacier: Glacier de St. Sorlin, France. *Earth Surf. Process. Landf.* 33 (13):1931–1947. <http://dx.doi.org/10.1002/esp.1635>.
- Ryan, J.C., Hubbard, A.L., Box, J.E., Todd, J., Christoffersen, P., Carr, J.R., Holt, T.O., Snooke, N.A., 2015. UAV photogrammetry and structure from motion to assess calving dynamics at Store Glacier, a large outlet draining the Greenland ice sheet. *Cryosphere* 9:1–11. <http://dx.doi.org/10.5194/tc-9-1-2015>.
- Smith, M.W., Vericat, D., 2015. From experimental plots to experimental landscapes: topography, erosion and deposition in sub-humid badlands from Structure-from-Motion photogrammetry. *Earth Surf. Process. Landf.* 40 (12):1656–1671. <http://dx.doi.org/10.1002/esp.3747>.
- Smith, M.W., Carrivick, J.L., Quincey, D.J., 2015. Structure from motion photogrammetry in physical geography. *Prog. Phys. Geogr.* 40 (2):1–29. <http://dx.doi.org/10.1177/0309133315615805>.
- Sund, M., Eiken, T., Hagen, J.O., Kääh, A., 2009. Svalbard surge dynamics derived from geomorphic changes. *Ann. Glaciol.* 50 (52), 50–60.
- Tonkin, T.N., Midgley, N.G., 2016. Ground-control networks for image based surface reconstruction: an investigation of optimum survey designs using UAV derived imagery and structure-from-motion photogrammetry. *Remote Sens.* 8 (9):786. <http://dx.doi.org/10.3390/rs8090786>.
- Tonkin, T.N., Midgley, N.G., Graham, D.J., Labadz, J.C., 2014. The potential of small unmanned aircraft systems and structure-from-motion for topographic surveys: a test of emerging integrated approaches at Cwm Idwal, North Wales. *Geomorphology* 226:35–43. <http://dx.doi.org/10.1016/j.geomorph.2014.07.021>.
- Tonkin, T.N., Midgley, N.G., Cook, S.J., Graham, D.J., 2016. Ice-cored moraine degradation mapped and quantified using an unmanned aerial vehicle: a case study from a polythermal glacier in Svalbard. *Geomorphology* 258:1–10. <http://dx.doi.org/10.1016/j.geomorph.2015.12.019>.
- Westoby, M.J., Brasington, J., Glasser, N.F., Hambrey, M.J., Reynolds, J.M., 2012. 'Structure-from-Motion' photogrammetry: a low-cost, effective tool for geoscientific applications. *Geomorphology* 179:300–314. <http://dx.doi.org/10.1016/j.geomorph.2012.08.021>.
- Westoby, M.J., Dunning, J., Hein, A.S., Woodward, J., Mölg, N., Paul, F., Sugden, D.E., 2016. Inter-annual surface evolution of an Antarctic blue-ice moraine using multi-temporal DEMs. *Earth Surf. Dyn.* 3:1317–1344. <http://dx.doi.org/10.5194/esurf-4-515-2016>.
- WGMS, 2015. Global Glacier Change Bulletin No. 1 (2012–2013). In: Zemp, M., Gärtner-Roer, I., Nussbaumer, S.U., Hüsler, F., Machguth, H., Mölg, N., Paul, F., Hoeszle, M. (Eds.), *ICSU(WDS)/IUGG(IACS)/UNEP/UNESCO/WMO. World Glacier Monitoring Service*, Zurich, Switzerland (230 pp.). 10.5904/wgms-fog-2015-11.